Electrochromism of Highly Doped Nanocrystalline SnO_2:Sb

U. zum Felde, M. Haase,* and H. Weller

Institut für Physikalische Chemie, Universität Hamburg, Bundesstrasse 45, D-20146 Hamburg, Germany

Received: March 15, 2000; In Final Form: July 2, 2000

The electrochromic effect of layers of nanocrystalline tin dioxide highly doped with antimony has been investigated in detail, using chronoamperometry, cyclic voltammetry, potential-dependent IR spectroscopy and UV−vis spectroscopy. It is shown that two different mechanisms are responsible for the color changes observed upon negative polarization of porous SnO_2:Sb nanocrystal layers. Injection of electrons via the back contact increases the plasma absorption of the material, which has its maximum intensity in the near-infrared region. This increase is accompanied by a strong increase of the electrical conductivity of the layer, indicating that the grain boundary potentials of the nanoparticle layer decrease at negative potentials applied. In the presence of small ions such as Li^+ or in protic electrolytes such as water, insertion of Li^+ and H^+ takes place, resulting in an additional color change mainly in the visible. The rate of the color changes is mainly determined by the conductivity of the substrate. Very fast coloration and decoloration is observed ($t_{1/2} < 10$ ms) if the particle layer is deposited onto highly conductive substrates such as platinum.

Introduction

Tin dioxide doped with antimony (ATO)[1] or fluorine (FTO)[2] belongs to the group of n-conductive oxides,[3] like the well-known ITO[4] (indium oxide doped with tin). If tin ions in tin dioxide are substituted by antimony, shallow electron donor levels are formed which are ionized at room temperature.[5] At doping levels of about 2 to 7% antimony, a degenerate semiconductor is formed displaying high electrical conductivity.[1,6,7] Because the number density of free conduction band electrons is lower than in metal elements, the onset of the plasma absorption of the free carriers is located in the near-infrared[8] rather than in the UV. Therefore, coatings of SnO_2:Sb (and SnO_2:F) are transparent for visible light and are widely used as transparent conductors in optoelectronic devices. Moreover, the coatings are used as heat shields,[9] because the high absorption coefficient of the plasma excitation renders them highly reflective for IR radiation. The IR absorption and the electrical conductivity of these films can be reasonably well described by applying simple Drude theory for a free electron gas.[10,11] Within this theory, the IR spectrum only depends on the concentration and the mean free path of the carriers. The latter two quantities also determine the conductivity of the layer if scattering of the electrons at grain boundaries is negligible. However, strong scattering at grain boundaries is often observed[12] in films of these materials because they are composed of particles in the nanometer size regime and their morphology is strongly influenced on the method of preparation.[13]

Antimony-doped tin dioxide is also used as catalyst for the selective oxidation of olefins.[14,15] These catalysts contain a much higher amount of antimony and display a lower electrical conductivity than the conductive films. At high antimony levels (above ∼4−7%) it is observed that an increasing amount of antimony in the oxidation state 3+ is incorporated into the lattice.[16,17] The latter is believed to be the reason for the decreased n-conductivity of the material.

More recently, the spectroelectrochemical properties of nanoporous electrodes prepared by spin coating colloidal SnO_2:Sb onto ITO-coated glass substrates have been investigated. Injection of electrons via the back contact results in a reversible color change of the material, i.e., an electrochromic effect.[18,19] The observed changes of the optical density at a wavelength of 650 nm, are $\Delta OD = 0.012$ and $\Delta OD = 0.15$ for a layer thickness of 0.284 μm[18] and 2.5 to 3.0 μm,[19] respectively. The absorption clearly scales with the number of electrons injected. However, the values of the corresponding coloration efficiency, defined as the geometrical area for which a change in optical density of $\Delta OD = 1$ is achieved by the injection of 1 coulomb, are quite different, i.e., $\eta(\lambda = 650\ \text{nm}) = 3\ \text{cm}^2/\text{C}$[18] and $\eta(\lambda = 650\ \text{nm}) = 23\ \text{cm}^2/\text{C}$,[19] respectively.

Boschloo and Fitzmaurice[19] pointed out that a space charge layer builds up at the surface of highly n-doped colloidal particles leading to depletion of electrons in the surface region. In porous electrodes composed of nanoparticles, the thickness of this depletion layer varies with the electrode potential, i.e., the charge injected into the electrode.

In this paper, we investigated the electrical conductivity and the IR absorption of the nanocrystalline SnO_2:Sb electrodes as a function of applied potential. We verify that the increase in conductivity observed at negative potentials is caused by an increase of the electron mobility rather than in increase of electron density in the particles. Moreover, we show that insertion of small cations into the crystal lattice can take place and that this insertion reaction contributes to the electrochromic effect.

Experimental Section

Preparation. Colloidal tin antimony oxide was prepared by the coprecipitation method[20−22] as reported recently.[23]

The molar ratio of tin and antimony in the dialyzed colloids was determined by atomic absorption spectroscopy (AAS) and was found to be equal to the ratio employed in the synthesis.

Layers of nanocrystalline tin dioxide have been prepared by spin coating at 2500 rpm quartz substrates with concentrated colloidal solutions. The latter were prepared by adding 1% of glycerin to each colloid and concentrating the colloids by a factor of about 4 using a rotary evaporator. Prior to deposition,

10.1021/jp0010031 CCC: $19.00
Published on Web 09/19/2000

500 μl of 25% ammonia was added under vigorous stirring to the highly viscous solution, which was then passed through a 0.2 μm filter. Spin coating was repeated about 10 times in order to obtain sufficiently thick layers. After each deposition step the layers were heated to 500 °C for 5 min. For comparison, we also prepared layers which were heated to 150 °C only. The thickness of the layers was determined with an alpha-step 200 profilometer (Tencor Instruments).

The conductivity of the layers was measured by the standard four-point method.[24]

Powders of nanocrystalline tin dioxide were prepared by removing the solvent of the respective colloidal solution with a rotary evaporator (bath-temperature of 50 °C). After drying at 100 °C in air, the residue was ground in a mortar. A portion of each powder sample was additionally heated to 500 °C in air for 1 h in an oven. Upon heating the brownish color of the doped samples changed to bluish, in accordance with observations made by others.[20]

The powder X-ray diffraction patterns of the materials are identical to those recently published [23] and indicate the absence of other phases than cassiterite.

Electrochemical and Spectroelectrochemical Measurements. A three-electrode cell with flat quartz windows was utilized for spectroelectrochemical measurements as well as cyclic voltammetry, chronoamperometry, and impedance measurements. A nanocrystalline SnO_2:Sb electrode and a large area platinum foil were used as working electrode and counter electrode, respectively. Measurements were performed either in an aqueous 3 M KCl electrolyte or in anhydrous propylene carbonate containing 0.1 M $LiClO_4$ or 0.1 M $N(C_4H_9)_4ClO_4$. Before use, propylene carbonate was dried over activated 0.5 nm molecular sieves for 5 days. An Ag/AgCl/KCl electrode ($E = +0.20$ V vs NHE) was used as reference electrode in aqueous electrolytes, whereas an Ag/Ag^+ electrode ($E = +0.80$ V vs NHE) was applied in aprotic electrolytes. All potentials given in the figures are reported against normal hydrogen electrode. Before each measurement the solution was purged with nitrogen to remove dissolved oxygen. All electrochemical studies were carried out with a Solartron Schlumberger ECI 1286 potentiostat.

For impedance measurements the potentiostat was connected to a Solartron Schlumberger FRA 1255 HF frequency response analyzer. An alternating voltage of 5 mV amplitude was superimposed on a dc potential, the voltage covering a frequency range from 0.1 Hz to 30 kHz. Equivalent circuit simulations were performed using software ("equivalent circuit") of the university of Twente, The Netherlands.

Potential Dependence of Electrical Conductivity. Electrodes prepared by depositing nanocrystalline SnO_2:Sb onto quartz substrates were used to measure the dependence of the infrared absorption and conductivity of SnO_2:Sb on electrode potential. The electrode was fixed in an electrochemical cell containing an aqueous 3 M KCl electrolyte and an open circuit potential in the range of $E = 0.07$ V, and $E = 0.92$ V was applied. The conductivity of the SnO_2:Sb layer itself was high enough to achieve polarization of the electrode. The electrode was removed from the cell, cleaned, and its infrared absorption and its conductivity were measured. After these measurements, the open circuit potential of the electrode was determined again. In the chosen potential range the potential shift during the absorption and conductivity measurement was smaller than 30 mV. At potentials more negative than $E = 0.07$ V electrochemical reduction of oxygen caused a loss of electronic charge. A large shift was also observed at potentials more positive than $E = 0.92$ V, probably caused by the oxidation of adsorbed hydroperoxide ions.

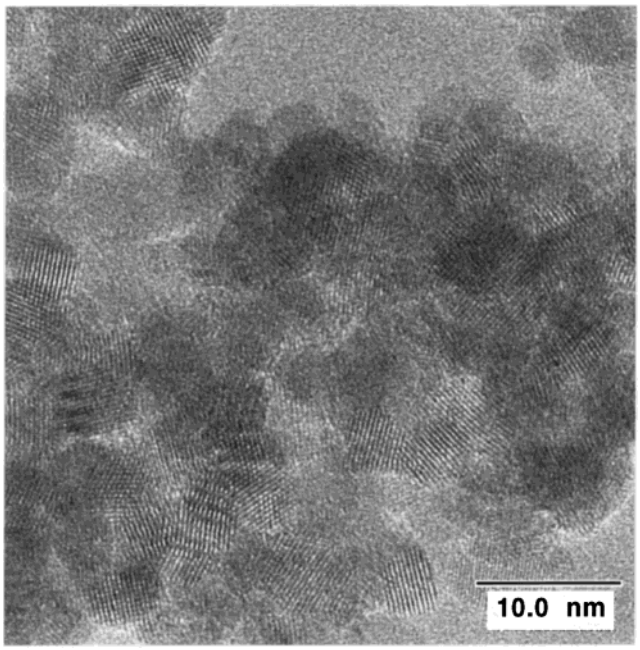

Figure 1. High-resolution TEM image of SnO_2:Sb nanocrystals (9.1% Sb) after heating to 500 °C for 1 h.

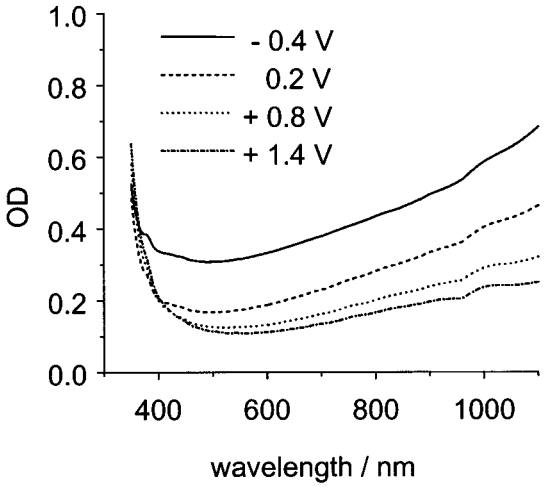

Figure 2. Absorption spectra of a nanoporous SnO_2:Sb electrode in aqueous 3 M KCl electrolyte as a function of applied potential.

Transmission Electron Microscopy. High-resolution transmission electron micrographs of the particle layers were taken using a Philips CM 300 UT electron microscope (300 kV acceleration voltage) equipped with a CCD camera (Gatan, model no. 694).

Results and Discussion

TEM Images. High-resolution transmission electron micrographs (Figure 1) of the SnO_2:Sb layers show an open network of interconnected nanocrystals with particle diameters ranging from 4 to 8 nm. Lattice fringes are observed for most particles, proving their high crystallinity. Measurements of the layer capacitance confirm a large inner surface area, as will be discussed below.

In contrast to dense layers of SnO_2:Sb, the nanoporous SnO_2:Sb electrodes show a pronounced electrochromic effect. Figure 2 shows the UV−vis absorption spectra of such an electrode in an aqueous electrolyte (3 M KCl_{aq}, pH 7), polarized at various

potentials. At positive potentials the SnO_2:Sb layer is colorless, whereas at negative potentials the electrode turns blue. Changing the electrode potential from $E = +1.4$ V to $E = +0.2$ V increases the absorption between 400 and 1100 nm by an almost constant factor. The strongest increase in absorption is observed in the red and infrared and is caused by Drude-type free carrier absorption, as will be discussed below. In our layers, absorption by free carriers is the dominant process contributing to electrochromism. At strongly negative potentials, however, the absorption increases in the blue as much as in the red, indicating an additional absorption process in the blue (Figure 2).

The intensity of the electrochromic effect depends on the thickness and the antimony content of the layer and is largest for SnO_2:Sb electrodes with an antimony content of $N_{Sb}/(N_{Sn} + N_{Sb}) = 16.7$ at. %. In this case, the difference in optical density between the colored and the bleached state is $\Delta OD = 0.5$ at 650 nm for a layer 2 μm thick.

The electrochromism of the nanoporous SnO_2:Sb electrode is fully reversible and very stable, if the electrode is cycled between $E = -0.4$ V and $E = +1.4$ V. At potentials more positive than $E = +1.4$ V electrochemical oxidation of the electrolyte takes place, whereas potentials more negative than $E = -0.4$ V lead to the evolution of hydrogen and destruction of the layer by reduction of tin ions to metallic tin. By keeping the electrode potential between -0.4 V and $+1.4$ V, however, we have been able to cycle our electrodes more than 10^6 times between the colored and bleached state without losing coloration efficiency. The coloration efficiency of our 2 μm thick SnO_2:Sb(16.7%) electrodes is $\eta = 18$ cm^2/C.

By potential step experiments we determined the kinetics of the electrochromic color change and the accompanying flow of current I and charge Q. The observed response time of the nanoporous SnO_2:Sb electrode strongly depends on the resistivity of the substrate. Figure 3 shows the kinetics of the absorption change at 650 nm as well as the $I - t$ and $Q - t$ response of a SnO_2:Sb(16.7%) layer deposited onto an FTO-coated glass substrate with a size of 2.3 cm^2 and a sheet resistance of 16 Ω/sq. Current densities and charge densities given in the figure refer to the *geometrical* area of the electrode. If the electrode potential is rapidly switched between $E = -0.4$ V and $E = +1.4$ V, coloration and bleaching take place within $t_{1/2} < 150$ ms. Coloration and bleaching are accompanied by high charging and decharging currents with single-exponential kinetics. The curve of the bleaching process follows the course of the charge density curve almost perfectly. Only at negative potential is the coloration current accompanied by a small leakage current. However, the observed decay curves are almost entirely determined by the RC characteristics of the substrate and do not reflect the kinetics of the electrochromic process itself. This is shown in Figure 4, displaying chronoamperometric measurements of a nanoporous SnO_2:Sb layer deposited onto a highly conductive platinum substrate. Coloration and decoloration of the electrode are much faster on platinum than on a FTO substrate. We observe a half-life of less than 10 ms, which is close to the time resolution of our apparatus. This shows that the electrochromic process itself is fast.

If a platinum substrate is used, evolution of hydrogen and destruction of the electrochromic layer is already observed at potentials more negative than $E = 0.0$ V, indicating that the electrolyte is in contact with the substrate. Obviously, the nanopores of the nanoparticle network are filled with electrolyte, and channels of interconnected nanopores reach from the surface of the layer to the surface of the substrate. The highly porous character of the nanocrystalline layer is also evident from its

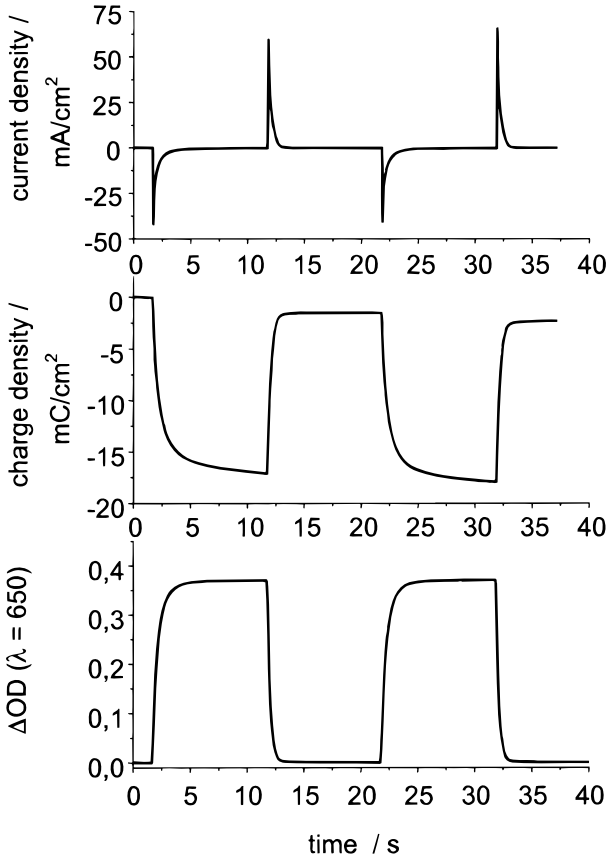

Figure 3. Current density, charge density, and change of absorption at a wavelength of $\lambda = 650$ nm of an SnO_2:Sb (16.7%) electrode as a function of time. The electrode in aqueous 3 M KCl electrolyte is switched between the colored state at $E = -0.4$ V and the bleached state at $E = +1.4$ V every 10 s (FTO substrate; $R_{sheet} = 16$ Ω/sq.).

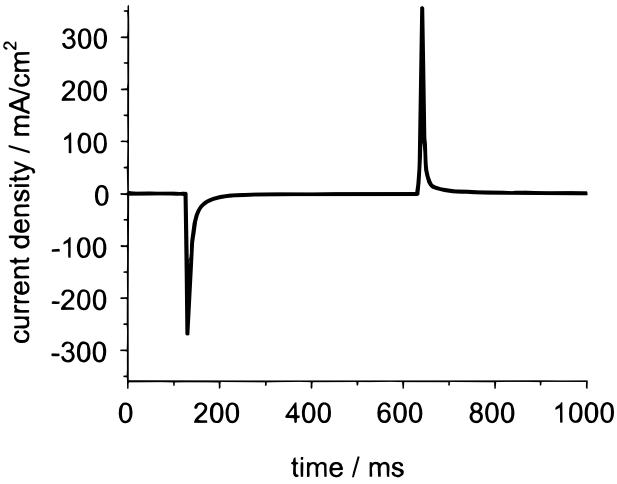

Figure 4. Current time response of an SnO_2:Sb (16.7%) electrode deposited on a platinum substrate. The electrode in aqueous 3 M KCl electrolyte is switched between $E = 0.0$ V and $E = +1.2$ V.

huge double-layer capacity. The charge densities given in Figure 4 for a 1 μm thick nanoporous layer are about 10^2-10^3 times higher than those of dense SnO_2:Sb layers.

Figure 5 shows cyclic voltammograms of a nanoporous SnO_2:Sb (16.7%) electrode immersed in anhydrous propylene carbonate, using tetrabutylammonium perchlorate and lithium perchlorate as supporting electrolyte, respectively. If the bulky tetrabutylammonium ion is used and if the electrode is well dried before use, the cyclic voltammogram shows a characteristic rectangular shape. The latter is typical of systems possessing a

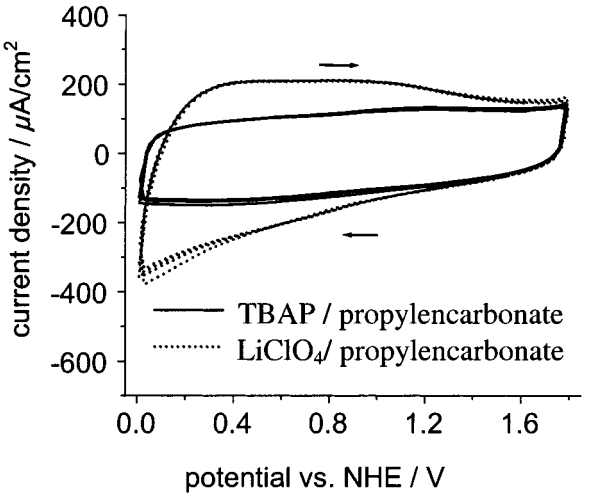

Figure 5. Cyclic voltammograms of an SnO_2:Sb (16.7%) electrode immersed in 0.1 M tetrabutylammonium perchlorate/propylene carbonate or in 0.1 M lithium perchlorate/propylene carbonate as electrolyte (sweep rate: $\upsilon = 50$ mV/s).

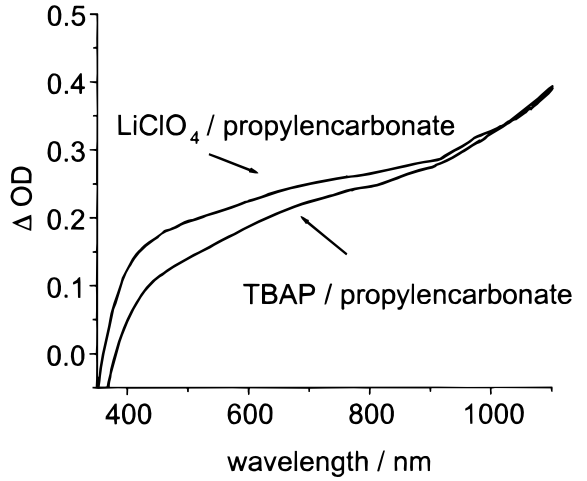

Figure 6. Change of absorption of the SnO_2:Sb (16.7 at. %) electrode (Figure 5) immersed in different electrolytes.

large double-layer capacitance[25] and corresponds to charging and decharging of the double-layers at the solid/liquid interface. In the presence of tetrabutylammonium cations this is the only process taking place because this ion is too large to be inserted into the SnO_2 lattice. The corresponding optical changes are given in Figure 6 and verify that the main part of the electrochromic effect is observed also in the absence of insertion reactions. As will be discussed in more detail below, this change in absorption is caused by conduction band electrons injected into the electrode via the back contact.[19] The negative charge of the injected electrons is compensated mainly by solvated ions in the pores.

The rectangular shape of the cyclic voltammogram is lost if the bulky tetrabutylammonium ions are replaced by small ions such as lithium or if a protic solvent like water is used rather than anhydrous propylene carbonate (Figure 5). In the presence of lithium ions or protons, high currents are observed at negative potentials, indicating that these ions are inserted into the crystal lattice of tin dioxide. Figure 6 shows that the insertion of lithium ions enhances the electrochromic coloration in the visible region of the spectrum only. The absorption in the IR remains almost unaffected. Similarly, the intercalation of protons in the presence of a protic solvent slightly increases the absorption in the visible (Figure 2).

A strong absorption in the blue is also observed[23] in tin dioxide containing both antimony (5+) and antimony (3+) and seems to be caused by an $Sb^{3+}-Sb^{5+}$ charge-transfer transition. In bulk SnO_2:Sb, the negative charge of free conduction band electrons is compensated by Sb^{5+}. Of course, reduction of Sb^{5+} ions to the much larger Sb^{3+} ions by conduction band electrons does not take place. However, the latter may occur at the particle surface, especially if the lattice constants in this layer are increased by the insertion of cations. In fact, Mössbauer measurements indicate that highly doped SnO_2:Sb contains Sb^{3+} ions which are mainly located at surface sites and grain boundaries.[17] Moreover, Sb^{3+} sites and Sn^{2+} sites at the particle surface are frequently discussed as reactive sites in SnO_2:Sb catalysts.[26] Therefore it may well be that electron injection accompanying the insertion of Li^+ or H^+ leads to the reduction of antimony atoms rather than a further increase of conduction band electrons. An analogue mechanism may be formulated for the reduction of Sn^{4+} to the large Sn^{2+} ion. Neglecting unusual oxidation states of tin and antimony, i.e., Sn^{3+} or Sb^{4+}, the most likely insertion reaction may therefore be formulated as

$$SnO_2{:}Sb + xLi^+ + xe^- \rightarrow Li_xSn^{IV}_{(1-x/2)}Sn^{II}_{x/2}O_2{:}Sb$$

$$SnO_2{:}Sb + xLi^+ + xe^- \rightarrow Li_xSnO_2{:}Sb^{V}_{(1-x/2)}Sb^{III}_{x/2}$$

The exact nature of the resulting intervalence transfer absorption is not yet known. However, hexachloroantimonate(III,V) salts, such as $(NH_4)_2Sn_{1-2x}Sb^{III}_xSb^{V}_xCl_6$, show a strong absorption band in the visible which has been attributed to an $Sb^{III}-Sb^{V}$ charge-transfer transition.[27] In the systems presented here, the contribution of insertion reactions to the total absorption change in the visible is not large and most of the electrochromic effect is attributed to Drude-type free carrier absorption, i.e., the plasma absorption of free electrons. Consequently, insertion reactions do not determine the rate of the electrochromic color change as it is the case for WO_3. The rate determining step is charging of the double layers which is a fast process due to the high mobility of solvated ion in the pores.

In the case of bulk metals and highly n-doped degenerate bulk semiconductors, the spectrum of the plasma absorption of free electrons has a steplike shape, the steepness of the absorption onset being determined by the mean free path of electrons in the material. The concentration (number density) of free electrons determines the spectral onset of the IR absorption. In the case of metal nanoparticles, however, this plasma absorption is compressed into a narrow absorption peak (plasmon polariton). The mean free path of electrons in the nanoparticles determines the width of the absorption peak, whereas the spectral position of the peak is determined by the number density of electrons and, to a lesser extent, by the dielectric function of the material embedding the nanoparticles. Figure 7 shows that the absorption peak of nanocrystalline SnO_2:Sb in fact shifts toward higher energies if the concentration of dopant and, hence, electrons in the particles is increased. From the peak maxima in Figure 7, the number density of electrons in the particles can be calculated. Using expressions given in[28-30] we obtain values of 5.6×10^{20} cm^{-3}, 6.3×10^{20} cm^{-3}, 7.4×10^{20} cm^{-3}, and 8.0×10^{20} cm^{-3} for particles doped with 4.8, 9.1, 16.7, and 20.6% of antimony, respectively. These values are typical of highly n-doped oxides[8] and are in accord with Hall measurements[31] of SnO_2:Sb layers indicating electron densities between 3×10^{20} and 8×10^{20} cm^{-3} for layers containing between 4 and 16% antimony. As expected, only a small fraction of antimony is ionized at high doping levels. The

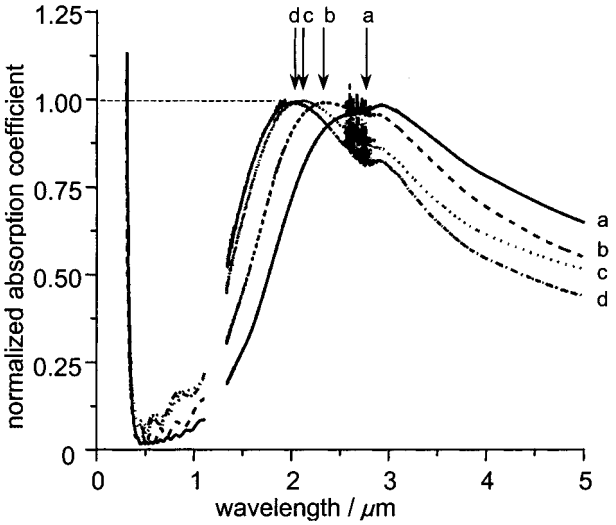

Figure 7. Normalized IR absorption spectra of SnO_2:Sb layers doped with (a) 4.8%, (b) 9.1%, (c) 16.7%, and (d) 20.6% antimony, respectively.

data show that the degree of ionization decreases from 42% for samples containing 4.8% of antimony to 25, 16, and 14% for samples doped with 9.1, 16.7, and 20.6% of antimony, respectively. Furthermore, the peak-shaped absorption indicates that the particles in the nanoporous layer must be electronically isolated from each other, for instance, by a poorly conductive shell around each particle. In fact, the surface layer of n-doped semiconductor nanoparticles is expected to exhibit a much smaller density of free electrons than the core of the particles, because semiconductor nanoparticles usually exhibit a large number of electron traps at the surface. For instance, some of the antimony(V) ions at the particle surface are believed to capture electrons, forming antimony(III) (see above). The presence of these and other immobile charges (e.g. charged surface states, adsorbed ions) at the solid/liquid interface form a space charge region near the particle surface, which, in the case of an n-doped semiconductor, is depleted of electrons.[32,33,19] Assuming a spherical particle and a uniform density of charges, the thickness $\Delta r = R - r$ of this depletion layer is related to the potential drop ϕ across the space charge layer by

$$\phi = \frac{eN_D}{6\epsilon\epsilon_0}\left(1 + \frac{2r}{R}\right)(R - r)^2 \qquad (1)$$

with N_D the number density of ionized antimony donor ions, e the elementary charge, ϵ the relative dielectric constant of the semiconductor, and ϵ_0 the dielectric constant of vacuum. It is important to note that only in the case of high doping levels is the depletion layer of the order of nanometers and, hence, smaller than the radius of the nanoparticle.[32]

If the nanoparticles form a porous electrode layer and the pores are filled with electrolyte, the potential drop ϕ and, hence, the thickness Δr of the depletion layer varies with the electrode potential applied.[19] This is schematically depicted in Figure 8, showing the spatial distribution of electrons inside a nanoparticle for two different values of ϕ. In fact, the infrared absorption of nanoporous SnO_2:Sb is affected by varying the electrode potential. For a SnO_2:Sb(16.7%) layer deposited onto quartz, Figure 9 shows how the IR absorption increases with the injection of electrons at negative polarization. This increase is the main contribution to the electrochromism of our layers because the IR absorption peak extents into the visible region (Figure 2) where the absorption change can be recognized by

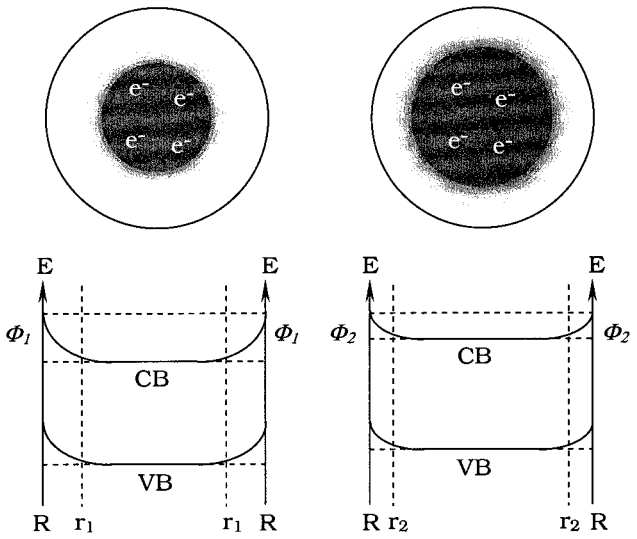

Figure 8. Particle volume containing conduction band electrons and thickness $\Delta r = R - r$ of the depletion layer at two different values for the potential drop ϕ at the particle surface.[31,32] If the nanoparticle is part of an electrode, ϕ varies with the applied electrode potential.[19]

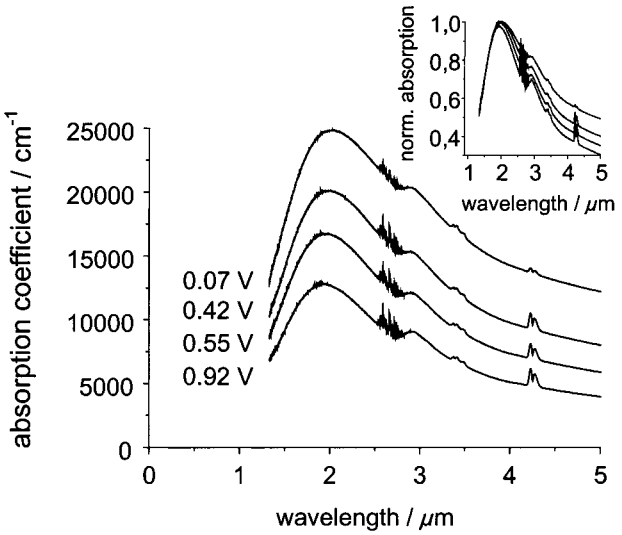

Figure 9. Absorption spectra in the near-infrared of an SnO_2:Sb (16.7%) electrode (substrate: quartz) as a function of applied potential (electrolyte: 3 M KCl_{aq}). Inset: same absorption curves normalized to the absorption peak at $E = +0.07$ V.

eye. In contrast to Figure 7, however, the increased number of electrons does not lead to a shift of the IR absorption peak indicating that the *concentration* of free electrons remains constant. Thus, varying the electrode potential must alter the *volume* occupied by electrons by the same factor as the *number* of electrons. This is exactly what the model of the space charge layer predicts as can be shown as follows. The number of free electrons in the core of each particle is

$$n_e = \frac{4\pi}{3}N_D r^3 \qquad (2)$$

whereas the charge stored in the depletion layer is given by

$$Q = \frac{4\pi}{3}eN_D(R^3 - r^3) \qquad (3)$$

According to eq 1 the radius r of the volume occupied by electrons changes from r_1 to r_2 if the electrode potential is altered in such a way that the potential drop changes from ϕ_1 to ϕ_2

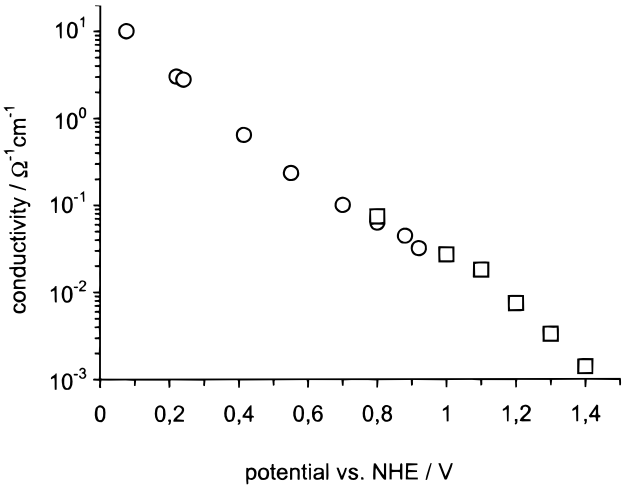

Figure 10. Electrical conductivity of an SnO_2:Sb (16.7%) electrode deposited on quartz as a function of applied potential. ○: Conductivity as measured with the four-point method. □: Conductivity as calculated from the impedance data shown in Figure 12.

(see also Figure 8). This alters the charge stored in the space charge layer by

$$\Delta Q = Q(r_1) - Q(r_2) = \frac{4\pi}{3} eN_D(r_1^3 - r_2^3) \qquad (4)$$

If the new electrode potential applied is more negative than the potential before, electrons are injected into the nanoparticles via the back-contact, the charge of these electrons corresponding to $-\Delta Q$. Hence, the number of electrons injected into the nanoparticle is $\Delta n_e = \Delta Q/e$, and the total number of free electrons in the particle is given by

$$n_e(\phi_2) = n_e(\phi_1) + \Delta n_e = \frac{4\pi}{3} N_D r_2^3 \qquad (5)$$

Because these electrons occupy a particle volume of $V(\phi_2) = (4/3)\pi r_2^3$, the number density of electrons is $n_e(\phi_2)/V(\phi_2) = N_D$, i.e., the same as before. Therefore, the *concentration* of free conduction band electrons in the particles is solely given by the number density of ionized donor ions and is *independent* of the electrode potential applied. However, changing the electrode potential *does* alter the volume occupied by electrons by $V(\phi_2)/V(\phi_1) = (r_2/r_1)^3$, in accord with the spectra given in Figure 9.

The inset of Figure 9 displays the absorption spectra of the main part of the figure after normalization at the peak intensity. Clearly, the absorption intensity at the low energy side of the absorption peak increases at negative electrode potentials. This asymmetric broadening of the absorption peak is typical of systems of metal particles where the interaction of the electron clouds of neighboring particles is not negligible.[28,30] In fact, at negative electrode potentials a stronger interaction must be expected because the thickness of the depletion layer of each particle decreases.

A thinner depletion layer should also lead to an increased electrical conductivity of the nanoporous layer, since the potential barriers between the particles are reduced. In fact, the electrical conductivity $\sigma = e\mu_e N_e$ of the layer increases exponentially with decreasing electrode potential (Figure 10). Because the IR spectra in Figure 9 show that the electron density N_e remains constant, it must be concluded that this increase in conductivity is caused solely by an increased electron mobility μ_e. This conclusion can be verified independently by impedance spectroscopy.

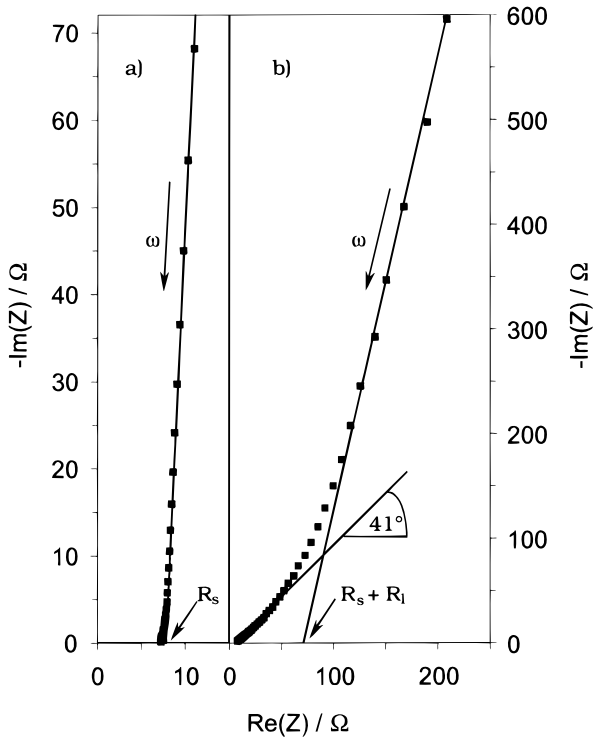

Figure 11. Nyquist plots of an SnO_2:Sb (16.7%) electrode in 3 M KCl_{aq} at different electrode potentials: (a) $E = +0.6$ V; (b) $E = +1.4$ V. The SnO_2:Sb layer is deposited onto a conductive FTO-coated glass substrate.

Parts a and b of Figure 11 display impedance spectra (Nyquist plots) of the SnO_2:Sb electrode recorded at electrode potentials of $E = +0.6$ V and $E = +1.4$ V, respectively. The impedance spectrum at $E = +0.6$ V is characterized by a straight line with a slope of almost 90°. This linear behavior is characteristic of the impedance of a simple RC element and shows that the impedance of the electrode is determined by two quantities only, its resistance R and its capacitance C. Note, that R is the total resistance of the electrode including the resistance R_l of SnO_2:Sb layer, the resistance R_s of the FTO-coated substrate, and the electrolyte. From the data points on the linear part of the spectrum, the capacitance of the electrode layer can be calculated. For the calculations, a constant phase element (CPE) was included in order to account for the slight deviation from a slope of 90°. Nevertheless, the capacitance C of the porous layer was found to depend only weakly on the frequency ω. The resistance R of the electrode is given by the intersect of the straight line with the x axis. In the potential range between $E = -0.4$ V and $E = +0.6$ V very similar impedance spectra are observed from which identical values for the resistance are calculated ($R_s = 7.7\ \Omega$). This is expected, because, due to the high conductivity of the layer in this potential range (Figure 10), the total resistance of the electrode is determined mainly by the resistance R_s of the conductive substrate and the leads.

At more positive potentials, the shape of the impedance spectrum starts to change. Part b of Figure 11 shows the spectrum at $E = +1.4$ V, i.e., at a strongly positive potential. Again, a steep line is observed at low frequencies ω. With increasing frequency, however, the impedance spectrum shows a transition to a second linear part, having a slope of about 45°. The latter is typical of a Warburg impedance arising from the diffusion of electroactive species. Impedance spectra consisting

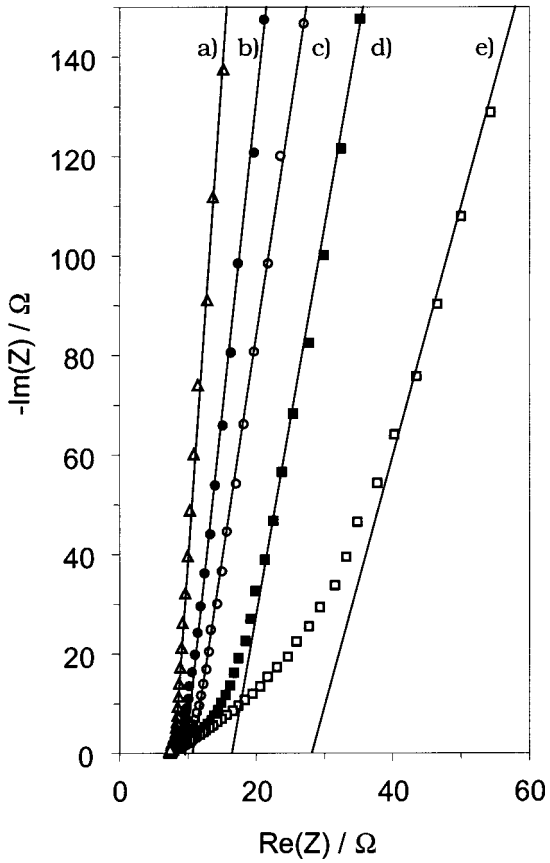

Figure 12. Nyquist plots of an SnO_2:Sb (16.7%) electrode in 3 M KCl_{aq} as a function of the applied potential: (a) $E = +0.8$ V; (b) E = +1.0 V; (c) $E = +1.1$ V; (d) $E = +1.2$ V; (e) $E = +1.3$ V. The SnO_2:Sb layer is deposited onto a conductive FTO-coated glass substrate.

of two linear parts, one with a slope close to 45° and the second with a slope close to 90° have been also observed for other thin solid electrodes and are in accord with the finite-length diffusion model for thin layers introduced by C. Ho, I. D. Raistrick, and R. A. Huggins.[34] In impedance measurements, the diffusion length of the electroactive species depends on the frequency ω of the alternating voltage, since the charge carriers diffuse to the opposite direction as soon as the polarity of the voltage is reversed. At high frequencies, the diffusion length is much smaller than the thickness d of the layer. As a result, a Warburg-like impedance typical of diffusion processes of mobile charge carriers is observed. At low frequencies, however, the charge carriers reach the back-contact and a similar behavior is observed as for the impedance spectrum given in part a. From the linear part of this region, the low-frequency capacitance C and resistance R are obtained[34] by the same method described above for the impedance spectrum measured at $E = +0.6$ V.

Similarly, values of C and R are determined for electrode potentials between $E = +0.8$ and $E = 1.2$ V from the impedance spectra given in Figure 12. In each case, the layer resistance R_l is obtained by subtracting $R_s = 7.7\ \Omega$ from the total resistance R. All values are summarized in Table 1.

The movement of the charge carriers through the layer to the back contact depends on their diffusion coefficient D. The latter is given by the resistance of the layer R_l, its capacitance C, and the layer thickness l according to[34]

$$D = \frac{l^2}{3C_lR_l} \qquad (6)$$

TABLE 1: Diffusion Coefficient D_e, Electron Mobility μ_e, and Conductivity σ of the SnO_2:Sb Layer as Calculated from the Resistance R_l and the Capacity C_l of the Electrode at Various Potentials E

E [V]	R_l/Ω	C_l/mF	$D_e/10^{-7}$ cm²/s	$\mu_e/10^{-5}$ cm²/Vs	$\sigma/10^{-3}$ Ω^{1-}cm^{-1}
+ 0.8	0.5	1.78	150	58	74
+ 1.0	1.8	1.38	54	21	27
+ 1.1	3.2	1.17	36	14	18
+ 1.2	9.3	0.97	15	5.8	7.4
+ 1.3	25	0.81	6.6	2.6	3.3
+ 1.4	72	0.67	2.8	1.1	1.4

[a] Values of R_l and C_l are determined from the impedance spectra given in Figures 11 and 12.

In a nanoprous network, three different diffusion processes may contribute to the impedance of the layer, i.e., the diffusion of electrons in the lattice, the diffusion of inserted ions in the lattice, and the diffusion of solvated ions inside the pores. For dense solids it has been presumed by P. J. Kulesza and J. A. Cox,[35] and shown for prussian blue electrodes by F. Vicente et al.[36,37] that the Warburg-like impedance can be related mainly to the diffusion of electrons if the mobility of the latter is much lower than the mobility of inserted ions. In our nanoporous electrodes, the charge of the electrons is compensated by ions in the pores which are filled with electrolyte. Because at room temperature the mobility of ions in solution is even much higher than of inserted ions in a solid, our impedance spectra are expected to be determined mainly by the diffusion of electrons in the solids. Therefore, the diffusion coefficient calculated above mainly describes the diffusion of electrons in the solid and is related to the electron mobility by the Einstein relation $\mu_e = (e/k_BT)$-D_e. Table 1 shows calculated values of D_e and μ_e at various potentials applied (thickness of the electrode $l = 2\ \mu$m). Clearly, the mobility increases from $E = +1.4$ V to $E = +0.8$ V by about a factor of 50. For potentials smaller than $E = +0.8$ V the determination of R_l becomes inaccurate, because R_l becomes much smaller than the sheet resistance of the substrate (Figure 12). Using a constant free electrons concentration of $N_e = 8.0 \times 10^{20}$ cm^{-3}, as determined from the peak position of the IR absorption curve, the electrical conductivity $\sigma = e\mu_eN_e$ of the layer can be calculated. In Figure 10 the calculated values are shown together with the conductivity values measured with the four-point method. The good agreement between the two data sets indicates that the potential dependence of the electron *mobility* is responsible for the change in conductivity rather than a change of the electron *concentration*. We therefore conclude that the conductivity of the nanocrystalline layer mainly depends on the thickness of the depletion layer which determines the mobility of the electrons.

Summary

In the present study we investigated the remarkable electrochromic effect of nanoporous antimony-doped tin dioxide. Electrodes are prepared by spin coating SnO_2:Sb colloids onto conductive substrates. The layers consist of interconnected nanocrystals showing the cassiterite crystal structure. Upon negative polarization, a reversible absorption change of $\Delta OD_{650\ nm} = 0.5$ is observed for 2 μm thick SnO_2:Sb-layers containing 16.7% antimony. This absorption in the visible and infrared part of the spectrum is mainly related to the plasma absorption of conduction band electrons in SnO_2:Sb nanoparticles.

Electrochemical in-situ UV−vis measurements of nanoporous layers deposited onto a metallic substrate exhibit a very short

response time ($t_{1/2}$ < 10 ms). Extended cycling between the colored and bleached state (10^6 cycles) does not deteriorate the electrochromic material.

Cyclic voltammetry measurements in an aprotic solvent containing tetrabutylammonium cations as supporting electrolyte revealed that insertion of cations into the solid is not necessary to observe the electrochromic coloration. Due to the large inner surface and because the SnO_2:Sb nanocrystals are in close contact with the electrolyte, charging of the double layers was sufficient to compensate the charge of the injected electrons and the rate of the electrochromic coloration is not determined by ionic diffusion in the crystal lattice.

In protic electrolytes or in aprotic electrolytes containing lithium ions, insertion reactions were observed at negative potentials. These insertion reactions are accompanied by additional absorption changes in the UV−vis presumably caused by intervalence charge-transfer transitions between tin or antimony cations of different oxidation states.

The IR absorption, the impedance, and the conductivity of the layers were measured at different electrode potentials. The results suggest the existence of a layer close to the surface of the nanoparticles that is depleted from free electrons. By changing the electrode potential, the thickness of this depletion layer can be varied. The latter changes the volume in the particles which is occupied by free electrons and affects the potential barriers between the nanoparticles.

Acknowledgment. We thank A. Kornowski for acquiring transmission electron micrographs.

References and Notes

(1) Shanthi, E.; Dutta, V.; Banerjee, A.; Chopra, K. L. *J. Appl. Phys.* **1980**, *51*, 6243.
(2) Shanthi, E.; Banerjee, A.; Dutta, V.; Chopra, K. L. *J. Appl. Phys.* **1982**, 53, 1615.
(3) Chopra, K. L.; Major, S.; Pandya, D. K. *Thin Solid Films* **1983**, *102*, 1.
(4) Hamberg, I.; Granqvist, C. G. *J. Appl. Phys.* **1986**, *60*, R 123.
(5) Fonstad, C. G.; Rediker, R. H. *J. Appl. Phys.* **1971**, *42*, 2911.
(6) Koch, H. *Phys. Status Solidi* **1963**, *3*, 1059.
(7) Herrmann, J.-M. J.; Portefaix, J.-L.; Forissier, M.; Figueras, F.;Pichat, P. *J. Chem. Soc., Faraday Trans. 1* **1979**, 1346.
(8) Bellingham, J. R.; Phillips, W. A.; Adkins, C. J. *J. Mater. Sci. Lett.* **1992**, *11*, 263.
(9) Frank, G.; Kauer, E.; Köstlin, H. *Thin Solid Films* **1981**, *77*, 107.
(10) Grosse, P. *Freie Elektronen in Festkörpern*; Springer-Verlag: Berlin, Heidelberg, 1979.
(11) Kittel, Ch. *Introduction to Solid State Physics*, 6th ed.; John Wiley & Sons: New York, 1986.
(12) Orel, B.; Lavrencic Stangar, U.; Opara, U.; Gaberscek, M.; Kalcher, K. *J. Mater. Chem.* **1995**, *5* (4), 617.
(13) Smith, A.; Laurent, J.-M.; Smith, D. S.; Bonnet, J.-P.; Clemente, R. R. *Thin Solid Films* **1995**, *266*, 20.
(14) Christie, J. R.; Taylor, D.; McCain, C. C. *J. Chem. Soc., Faraday Trans. 1* **1976**, *72*, 334.
(15) Timm, D. L.; Galbay, D. S. *Trans. Faraday Soc.* **1971**, *67*, 2782.
(16) Kojina, M.; Kato, H.; Gatto, M. *Philos. Mag. B* **1993**, *68* (2), 215−222.
(17) Berry, F. J.; Laundy, B. J. *J. Chem. Soc., Dalton Trans.* **1981**, 1442.
(18) Orel, B.; Lavrencic Stangar, U.; Kalcher, K. *J. Electrochem. Soc.* **1994**, *141*, L127.
(19) Boschloo, G.; Fitzmaurice, D. *J. Phys. Chem. B* **1999**, *103*, 3093.
(20) Vincent, C. A.; Weston, D. G. C. *J. Electrochem. Soc.* **1972**, *119* (4), 519.
(21) Crnjak-Orel, Z.; Orel, B.; Hodoscek, M.; Kaucic, V. *J. Mater. Sci.* **1992**, *27*, 313.
(22) Orel, B.; Lavrencic-Stangar, U.; Crnjak-Orel, Z.; Bukovec, P.; Kosec, M. *J. Non-Cryst. Solids* **1994**, *167*, 272.
(23) Rockenberger, J.; zum Felde, U.; Tischer, M.; Tröger, L.; Haase, M.; Weller, H. *J. Chem. Phys.* in press.
(24) van der Pauw, L.-J. *Philips Res. Rep.* **1958**, *13*, 1.
(25) Kastening, B.; Hahn, M.; Rabanus, B.; Heins, M.; zum Felde, U. *Electrochim. Acta* **1997**, *42*, 2789.
(26) Dusastre, V.; Williams, D. E. *J. Phys. Chem. B* **1998**, *103*, 6732.
(27) Atkinson, L.; Day, P. *J. Chem. Soc. A* **1969**, 2423.
(28) Kreibig, U.; Vollmer, M. *Optical Properties of Metal Clusters*; Springer-Verlag: Berlin, Heidelberg, 1995.
(29) Henglein, A. *J. Phys. Chem.* **1993**, *97*, 5457.
(30) Nütz, T.; zum Felde, U.; Haase, M. *J. Chem. Phys.* **1999**, *110* (24), 12142.
(31) Terrier, C.; Chatelon, J. P.; Roger, J. A. *Thin Solid Films* **1997**, *295*, 95.
(32) Albery, W. J.; Bartlett, P. N. *J. Electrochem. Soc.* **1984**, *131* (2), 315.
(33) Goossens, A. *J. Electrochem. Soc.* **1996**, *143* (6), L131.
(34) Ho, C.; Raistrick, I. D.; Huggins, R. A. *J. Electrochem. Soc.* **1980**, *127*, 343.
(35) Kulesza, P. J.; Cox, J. A. *Electroanalysis* **1998**, *10*, 73.
(36) Garcia-Jareno, J. J.; Navarro, J. J.; Roig, A. F.; Scholl, H.; Vicente, F. *Electrochim. Acta* **1995**, *40*, 1113.
(37) Garcia-Jareno, J. J.; Sanmatias, A.; Navarro-Laboulais, J.; Benito, D. Vicente, F. *Electrochim. Acta* **1998**, *43*, 235.